AD-A170 756 LIMITS OF PATTERN DISCRIMINATION IN HUMAN VISION(U) 1/1
YALE UNIV NEW HAVEN CT DEPT OF OPHTHALMOLOGY AND VISUAL SCIENCE J HIRSCH 03 FEB 86 AFOSR-TR-86-0369
UNCLASSIFIED F49620-83-C-0026 F/G 5/10 NL

END
DATE FILMED
9-86
DTIC

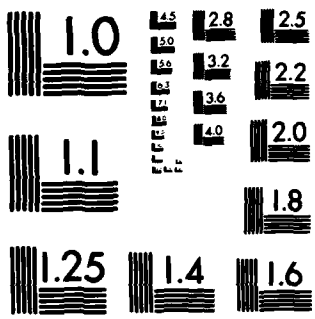

(2)

SECURITY CLASSIFICATION OF THIS PAGE (When Data Entered)

REPORT DOCUMENTATION PAGE

READ INSTRUCTIONS BEFORE COMPLETING FORM

1. REPORT NUMBER: AFOSR-TR- 86-0569
2. GOVT ACCESSION NO.
3. RECIPIENT'S CATALOG NUMBER

4. TITLE (and Subtitle): Limits of Pattern Discrimination in Human Vision
5. TYPE OF REPORT & PERIOD COVERED: FINAL TECHNICAL REPORT January 1983 - December 1985
6. PERFORMING ORG. REPORT NUMBER

7. AUTHOR(s): Joy Hirsch, Ph.D
Associate Professor
8. CONTRACT OR GRANT NUMBER(s): F49620-83-C-0026

9. PERFORMING ORGANIZATION NAME AND ADDRESS:
Yale University School of Medicine
Department of Ophthalmology and Visual Science
310 Cedar Street, New Haven, CT. 06510
10. PROGRAM ELEMENT, PROJECT, TASK AREA & WORK UNIT NUMBERS: 61102F 2313 A5

11. CONTROLLING OFFICE NAME AND ADDRESS:
Grants and Contracts
Sterling Hall of Medicine
333 Cedar St., New Haven, CT. 06510 DL
12. REPORT DATE: 3 February 1986
13. NUMBER OF PAGES: 28

14. MONITORING AGENCY NAME & ADDRESS (if different from Controlling Office): Same as 11
15. SECURITY CLASS. (of this report)
15a. DECLASSIFICATION/DOWNGRADING SCHEDULE

16. DISTRIBUTION STATEMENT (of this Report)

Approved for public release,
distribution unlimited

17. DISTRIBUTION STATEMENT (of the abstract entered in Block 20, if different from Report)

DTIC ELECTE AUG 1 1 1986 S D

18. SUPPLEMENTARY NOTES

19. KEY WORDS (Continue on reverse side if necessary and identify by block number)

Spatial Vision
Hyperacuity
Weber's Law
Pattern Discrimination

20. ABSTRACT (Continue on reverse side if necessary and identify by block number)

This investigation was focused on identification of various limits of human spatial discrimination, two-dimensional sampling properties of the retinal photoreceptor lattice, and the consequences for spatial vision. Highlights from this study are briefly listed below.

DD FORM 1 JAN 73 1473 EDITION OF 1 NOV 65 IS OBSOLETE

SECURITY CLASSIFICATION OF THIS PAGE (When Data Entered)

AD-A170 756

DTIC FILE COPY

86 8 8 078 11 FEB 1986

Foveal Spatial Discriminations are hyperacuity tasks; Results from these studies have shown that in human vision both spatial-frequency discrimination and line-separation discrimination (above 4 cycles/degree of visual angle) are hyperacuity tasks where performance far exceeds the resolution expected based on photoreceptor spacing. This observation had not been made before and serves to unify models of discrimnation and hyperacuity.

The spatial-frequency discrimination function ($\Delta f/f$ vs f) is segmented. Spatial-frequency and line-separation discrimination ($\Delta f/f$ and $\Delta s/s$) above approximately 2 (c/deg) is not a smooth function of spatial frequency (as previously assumed) but instead is regularly segmented about a constant value ($\Delta f/f$ is approximately 0.025). This characteristic of the discrimination function may reflect the engineering of Weber's Law as well as the existence of a neural scaling metric.

The discrimination segments can be related to retinal sampling. The segments in the spatial-frequency and line-separation discrimination functions are related to an underlying neural structure that reflects the sampling properties (center-to-center spacing) of the foveal mosaic. Each segment corresponds to a discrete level of performance that is either equal or proportional to photoreceptor spacing. This is a new approach to models of spatial vision.

Scaling mechanisms apply to low resolution tasks. The spatial-frequency discrimination function ($\Delta f/f$ vs f) below 2 c/deg also shows evidence for segmentation similar to the higher spatial frequency range - except that the fundamental unit is about 7 or 8 times the center-to-center spacing of foveal cones. This observation suggests that for low spatial frequency tasks (large spatial intervals) the effective sampling lattice may consist of receptive fields instead of photoreceptors. Accordingly, the notion of hyperacuity may be generalized to low resolution tasks where neural interpolation occurs not only on the photoreceptor sampling lattice to achieve hyperacuity, but also on receptive field sampling lattices to achieve lower resolutions.

The photoreceptor lattice is a highly ordered hexagonal array. The above findings and the apparent reflections of lattice sampling properties in spatial vision have led to an investigation of the primate lattice structure. An analysis strategy was developed to quantify the two-dimensional spatial (crystalline) quality of the primate photoreceptor lattice (digitized from electronmicrographies by Wm. H. Miller). This new technique has yielded an index of positional variance by accumulating expected and observed positional deviations over the lattice surface. The primate foveal lattice (contrary to prior proposals) was found to be an extremely regular and hexagonal (triangular) structure supporting the notion that the photoreceptor lattice could provide the primary source of geometrical information for the visual system. That is, neural representation of the lattice could provide a 'ruler' for spatial vision.

A hexagonal component exists in spatial discrimination. Both spatial frequency discrimination and vernier acuity (a classical hyperacuity task) show an orientation dependence that contains a component with hexagonal symmetry suggesting that the two dimensional sampling properties (hexagonal packing) of the photoreceptor mosaic are reflected in mechanisms of spatial vision.

A new 'metric' model of spatial vision is based on visual sampling. A Scaled Lattice Model of spatial vision based on alternative sets of neural scales fundamentally related to retinal sampling has been formally proposed. The model allows scale free spatial processing while retaining the advantages of linear maps and offers an alternative explanation for many spatial vision tasks such as types of separation discrimination and hypercuity.

Hirsch, Joy
F49620-83-C-0026

AFOSR-TR- 86-0569

TABLE OF CONTENTS

1. Research Objectives

The previous study was subdivided into five objectives. Each objective represented an approach to investigate the limits of human spatial discrimination and to relate the findings to the sampling properties of the photoreceptor array.

The five objectives are listed below.

Objective 1. To study how the limits of spatial frequency discrimination are related to hyperacuity performance and neural interpolation.

Objective 2. To study how spatial frequency discrimination varies as a function of stimulus orientation.

Objective 3. To determine the limits of spatial frequency discrimination for very low spatial frequencies.

Objective 4. To investigate the quality of the primate photoreceptor lattice and relate the structural properties of the foveal retinal mosaic to the 'neural metric' employed in hyperacuity tasks.

Objective 5. To develop a model of spatial discrimination based on spatial properties rather than contrast.

2. Status of the Research Effort

Objective 1: TO STUDY HOW THE LIMITS OF SPATIAL-FREQUENCY DISCRIMINATION ARE RELATED TO HYPERACUITY PERFORMANCE AND NEURAL INTERPOLATION.

The accuracy with which the human visual system is able to estimate positions of lines (as in the case of vernier acuity) exceeds the resolution of the photoreceptors mosaic. This extraordinary sense of image position requires some form of neural interpolation in order to achieve such a fine grained representation (Barlow, 1979, Westheimer, 1979, Fahle and Poggio, 1981). In recent years much attention has been given to the spatial frequency properties of the eye. However, the limits of suprathreshold frequency discrimination have not previously been related to the limits of separation discrimination.

Methods and Procedures for Objective 1

Stimuli were vertical sinusoidal spatial frequency gratings electronically generated on the face of a CRT (Tektronix 606, P31 phosphor). The gratings were calculated by a PDP 11/03 computer and stored in digital display generating hardware.

Sessions were controlled by the laboratory computer, and the data analysis followed each experimental session. The data were gathered over a period of 18 months in irregular order.

The observer initiated a trial by pressing a ready key. A trial consisted of a reference grating presented for 1.5 sec, an interstimulus interval of .75 sec, and a test grating presented for 1.5 sec. All stimuli were stationary with abrupt on and offsets, and the phases of both the test and reference gratings were independently randomized on each trial. Onsets of both reference and test gratings were cued by a tone. A response period followed the test stimulus and was indicated by a beep and an LED alphanumeric display located to the side of the screen.

The observer's task was to decide if the test grating had a higher or a lower spatial frequence than the reference grating. A two alternative forced choice method was employed where the observer signaled a 'high' or 'low' response by pressing the appropriate key on a response panel. Following each response a synthesized voice unit (Votrax VSK) replied either 'high', 'low', or 'same' indicating whether the test grating presented on that trial had been a higher spatial frequency, a lower spatial frequency, or the same spatial frequency as the reference grating.

Seven test gratings were employed during each session. Three were of lower spatial frequency than the reference grating, three were of higher spatial frequency than the reference, and one was the same spatial frequence as the reference. Test grating frequencies were chosen symmetrically about the reference frequency. All reference gratings were presented at 30% contrast. Prior to the sessions, a contrast matching experiment was done so that each test grating had the same apparent contrast as the reference grating.[4] In addition, on each trial the contrasts of both the test and reference gratings were given small random variations (between $\pm$ 1 db) to further ensure that no contrast cues existed. All test gratings were randomized and presented with equal probabilities. Each test grating was presented 50 times. A session consisted of 350 trials plus 20 initial practice trials that were excluded from the data analysis.

The probability of a 'high' response was fit to a cumulative normal distribution described by two parameters, f_c and Δf. The value of f_c is the frequency at which the probability of a 'high' response is .50, and Δf, the just discriminable difference (jnd) in spatial frequency, is proportional to the width of the normal distribution with a constant scale factor chosen so that the probability of a correct response is .75 when $f-f_c$ equals Δf. (Δf equals .68 times the standard deviation of the fitted normal distribution.) The fit was made using the method of maximum likelihood and also yielded estimates of the statistical errors for both parameters. The estimated error bars were verified by replicating a number of points over time. Chisquared values calculated for the fits indicated good agreement between the fit and the data in all cases, and f_c did not differ significantly from the reference frequency.

FINDINGS FOR OBJECTIVE 1:

1. Spatial-frequency discrimination and line-pair separation discrimination are hyperacuity tasks for spatial-frequencies (inverse separations) above 4 c/deg.

The spatial-frequency data for observer JH are plotted in terms of Δs (Figure 1a) and compared to the separation discrimination data shown in b. Also shown in Figure 1b are results of a similar line pair experiment previously reported by Westheimer (1979) (open symbols) which are consistent with our observations. From this figure it can be seen that the angular resolution Δs for both tasks is much smaller than the spacing between photoreceptors for medium and high spatial frequencies. (As a point of reference, the size of a photoreceptor is estimated to be about 30 secs of arc or .008 degrees.2)

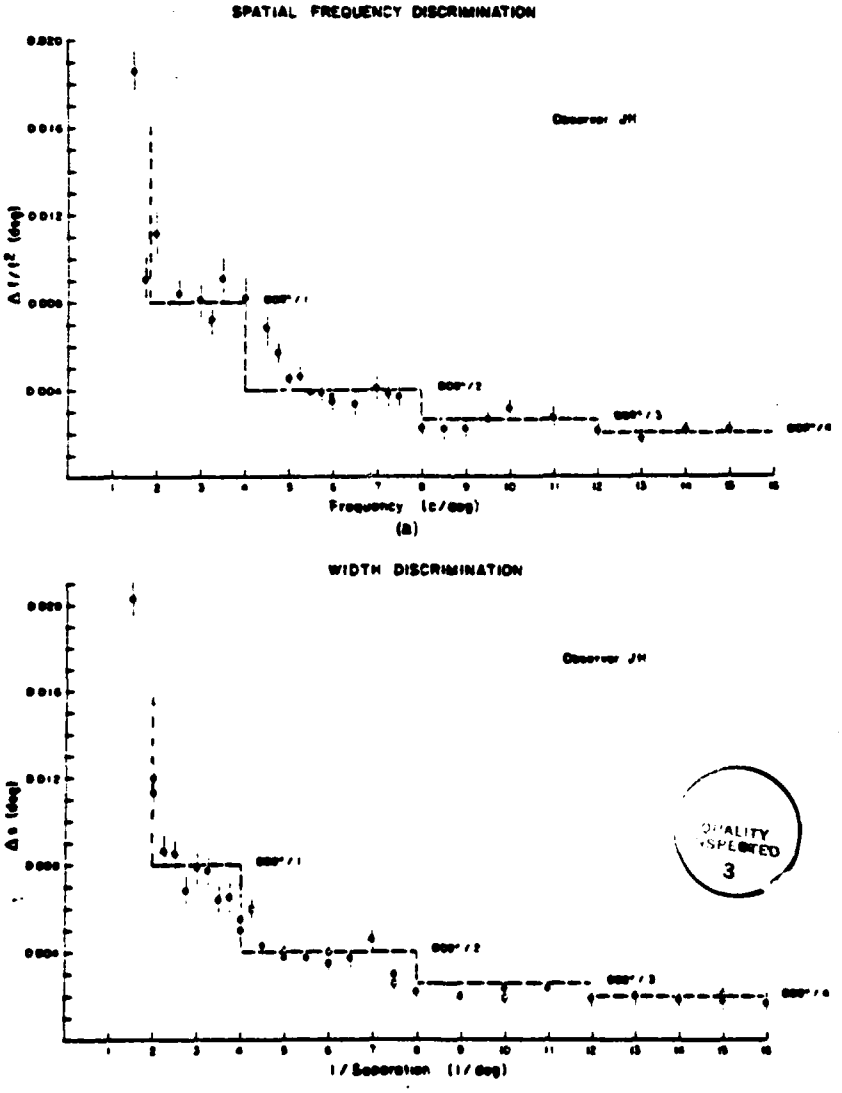

Figure 1. (from Hirsch, J. and Hylton, R. (1982) 'Limits of spatial-frequency discrimination as evidence of neural interpolatcn'. J. Opt. Soc. Am. 72, 1367-1374.)

2. Spatial-frequency discrimination is independent of field size for field sizes greater than 2 cycles

In another set of measurements all gratings were presented as described above except that the extent of sinusoidal modulation for both test and reference gratings in a particular session was restricted to a region of constant angular width less than the full screen. The phases were randomized as described above and the modulation was abruptly reduced to zero outside the display region. Both test and reference gratings remained centered in the four degree field.

Figure 2 shows $\Delta f/f$ as a function of the number of cycles in the reference grating for observer BA and spatial frequencies of 4, 8, and 12 cycles/deg. Similar results were found for observer JH. In all cases it can be seen that the $\Delta f/f$ function is independent of field size until the fied size becomes less than two cycles. The scatter in the data for field sizes of two cyles and above is consistent with the error bars on each point.

We interpret this as evidence that the spatial frequency discrimination was in fact done by measurement of the separation between two visual features separated by exactly one spatial cycle. In particular, if the task were based on measurement of the distance between two successive peaks, performance would degrade rapidly as field size became less than two cycles because a random sample of a sine wave becomes increasingly less likely to contain two intact peaks as the sample width decreases below two cycles. A sample containing only one cycle cannot contain two intact peaks.

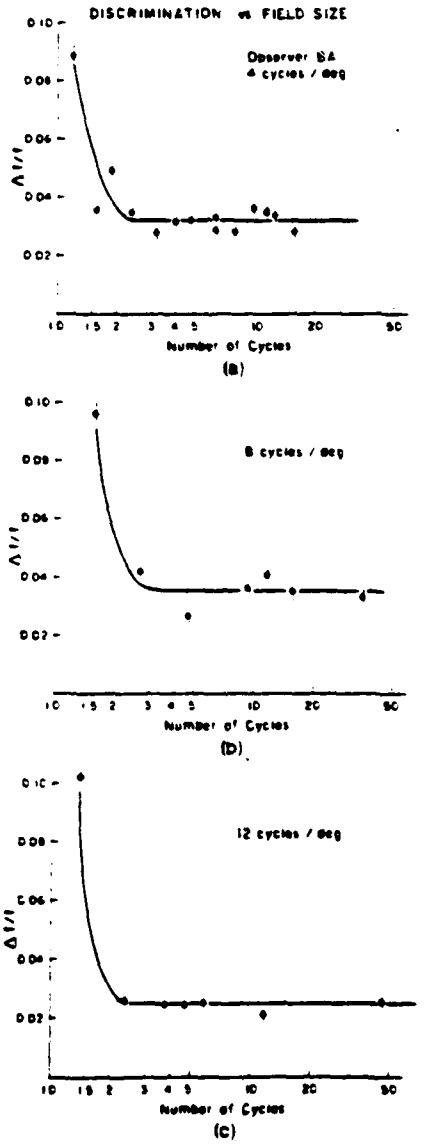

Fig. 2. Fractional ind in spatial frequency ($\Delta f/f$) as a function of field size (number of cycles in the reference grating) for observer BA at 4, 8, and 12 c/deg.

Figure 2. (From Hirsch, J. and Hylton, R. (1982) 'Limits of spatial-frequency discrimination as evidence of neural interpolation'. J. Opt. Soc. Am. 72:1367-1374).

3. Spatial-frequency discrimination and 2-line interval discrimination are not smooth functions of spatial-frequency or inverse separations

Discrimination of spatial frequencies

Three observers (JH, BA, and MM) with unimpaired vision participated in the experiment. Data from each are shown in Figure 3. Values of $\Delta f/f$ (where Δf is defined above and f is the reference frequency) are plotted against the reference frequency. Each point represents one session and errors on each point are estimates from the fitting procedure. The data are clearly not a smooth function of frequency but rather show a segmented structure for all observers. Further, the data are not well fit by a single straight line (chisquared confidence levels less than .05 in all three cases).

Examination of the data yields several significant characteristics of the $\Delta f/f$ vs f function. First, the $\Delta f/f$ function can be divided into several segments. The segments occur at approximately the same place for all observers, and are separated by transition regions where $\Delta f/f$ falls rapidly with spatial frequency. The transitions appear nearly regularly spaced in spatial frequency, repeating about every four cycles/deg. Peak values of $\Delta f/f$ are about the same for each segment across all observers, with a value of approximately .032. Within each segment $\Delta f/f$ rises with spatial frequency (following the transition), and the points are clustered around straight lines drawn through the origin. The slopes of these lines vary systematically from segment to segment. Disregarding the segmentation, it can be seen from Figure 3 that $\Delta f/f$ is essentially independent of spatial frequency. This observation suggests that over the range of spatial frequencies studied the visual system on the average achieves a resolution which is a constant fraction (approximately .025) of the size of the relevant visual characteristic.

Discrimination of separations between line pairs

This experiment was similar to the spatial frequency discrimination experiments described above except that a single pair of very thin vertical lines on a dark background was presented instead of a spatial frequency grating. The task for the observer was to decide if the separation between the test pair of lines was greater or less than the separation between the reference pair of lines. Deviations of test separations from reference separations were controlled to an accuracy of better than 10^{-4} degrees, and the center of each pair of lines was independently randomized around the center of the display by $\pm$ 1/4 of the reference separation. In all other respects, this experiment was the same as the spatial frequency experiments. Data from each session were analyzed as above to obtain estimates of the center separation, the jnd in separation Δs, and the error on each. The results for this experiment are shown for observer JH in Figure 3. The fractional resolution in separation, $\Delta s/s$, is plotted against the inverse of reference separation, 1/s.

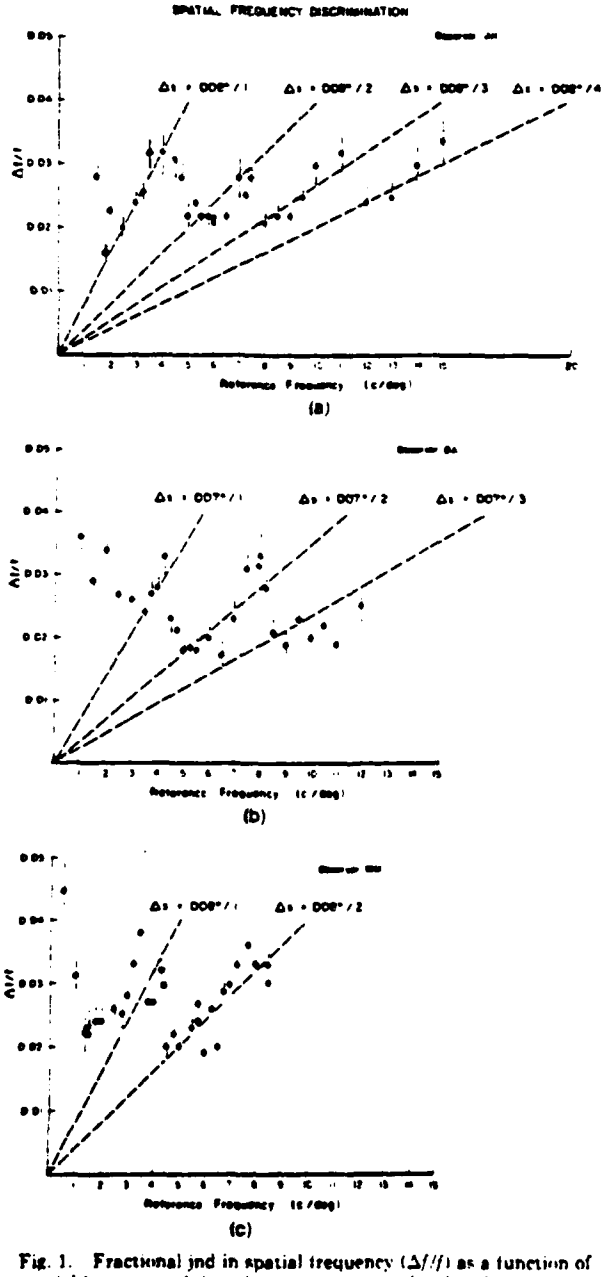

Fig. 1. Fractional jnd in spatial frequency ($\Delta f/f$) as a function of spatial frequency of the reference grating (cycles/deg) for observers JH, BA, and MM. The straight lines passing through the origin represent regions of constant angular jnd Δs. Determination of the lines is discussed in the text.

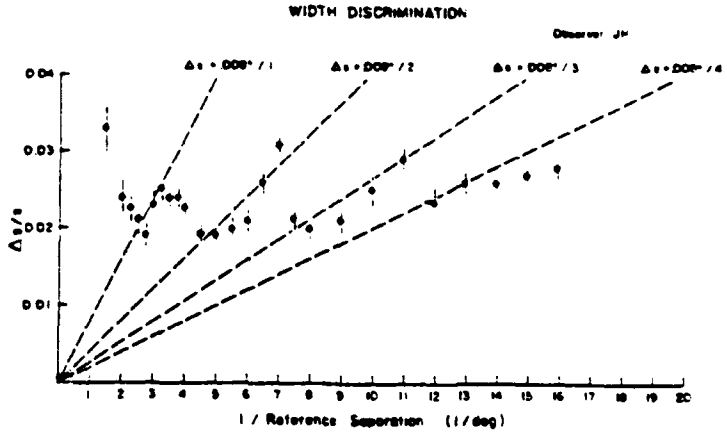

Fig. 3. Fractional jnd in separation ($\Delta s/s$) as a function of 1/reference separation (deg^{-1}). The straight lines passing through the origin represent the regions of constant angular jnd Δs as shown in Fig. 1.

Figure 3. (from Hirsch, J. and Hylton, R. (1982) 'Limits of spatial-frequency discrimination as evidence of neural interpolation.' J. Opt. Soc. Am. 72, 1367-1374.

4. The discontinuities in the discrmination function above 4 c/deg appear to be related to foveal photoreceptor spacing

The data shown in Figure 3 for spatial-frequency discrimination and line separation discrimination were fit to a family of straight lines passing through the origin. The slopes of the lines were equal to ε/n where n started at 1 and incremented by integers over the range of separations studied. The lines represent regions of constant jnd in separation, Δs.

Results of these studies for 3 observers and two types of experiments suggested that Δs for the first segment was approximately 0.008 deg for all cases. Since 0.008 degrees is also the angular substance of a foveal cone[2] we suggested that the accuracy of spatial separation discrimination for separations between about 1.5 to 4.0 deg^{-1} was equivalent to photoreceptor spacing.

For inverse separations and spatial frequencies above about 4 c/deg the jnd in separation Δs becomes progressively finer. For example by 8 c/deg the Δs is reduced by a factor of 2 and by 12 c/deg the Δs is reduced by a factor of 3.

These results inspired the notion that the photoreceptor spacing in the fovea may provide a type of geometrical ruler for spatial vision. Subsequent studies have tested various aspects of this notion.

5. The limit of spatial frequency discrimination is approximately 28 c/deg which corresponds to a separation discrimination of approximately 4 secs of arc

An experiment was performed to test the spatial-frequency limits of spatial-frequency discrimination. Methods were as described above except that test frequencies were matched for apparent contrast. Results are shown for observer JH and indicate that in general the average fractional jnd remains around 0.025 out to 28 c/deg beyond which this observer or no other in the lab could continue to make comparable spatial-frequency discrminations.

Continuation of the family of lines drawn through the origin with slopes equal to ε/n as discussed above suggests that at 28 c/deg the jnd in spatial-frequency discrimination $\Delta s = 0.008/7$ degrees (0.0011 degrees or approximately 4 seconds of arc.)

It appears that in order to keep the fractional jnd approximately constant the 'spatial ruler' of the visual system shifts to finer and finer spatial scales with increasing spatial frequency. In fact, from approximately 4 to 28 c/deg at least 7 levels of hyperacuity performance can be identified based on the fundamental foveal center-to-center spacing as the metric.

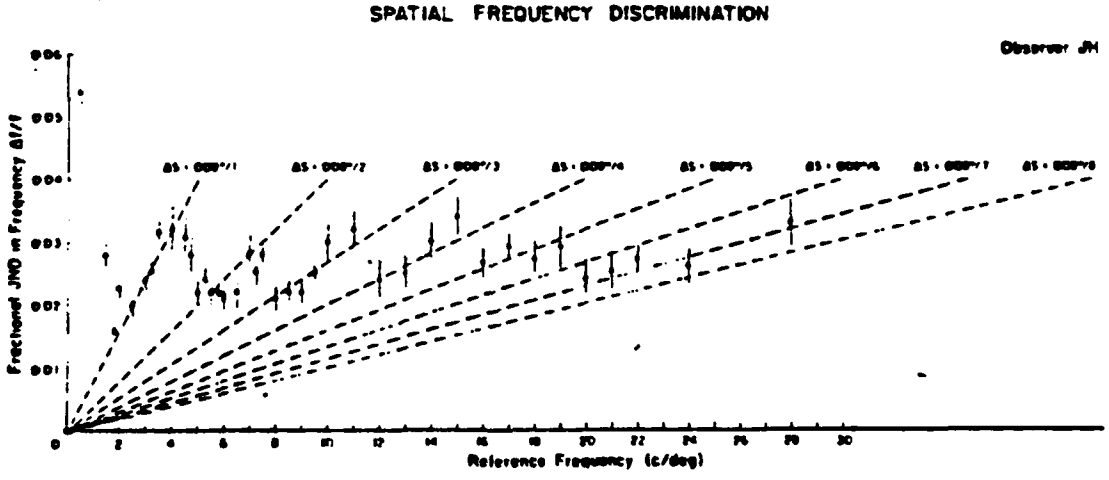

Figure 4. Similar to Figure 3 with spatial-frequencies extending to 28 c/deg. These data are presented in: Hirsch, J. and Hylton, R. (1984) 'Quality of the primate photoreceptor lattice and limits of spatial vision' Vison Res. 24, 347-355.

OBJECTIVE 2: TO STUDY HOW SPATIAL-FREQUENCY DISCRIMINATION VARIES AS A FUNCTION OF STIMULUS ORIENTATION.

In the above study we reported that discriminating between spatial frequency of suprathreshold sinusoidal gratings near and above four cycles/degrees (c/deg) is a task involving spatial hyperacuity, angular resolutions finer than the center-to-center spacing of foveal photoreceptors.4 Further, the magnitude of the hyperacuity thresholds were related to the center-to-center spacing of photoreceptors. We suggested that this relationship was due to a cortical representation of the image that directly reflected the organization of the retinal photoreceptor lattice. A logical consequence of this argument is that the two dimensional properites of the coritcal mechanisms which process spatial information should also reflect the two dimensional organization of the photoreceptor lattice.

Methods and Procedures for Objective 2

Two different tasks were employed: discriminating between spatial frequencies of suprathreshold sinusoidal gratings and discrminating the direction of the vernier offset of two narrow lines. In both experiments stimuli were electronically generated on an oscilloscope screen (Tektronix 606). A single experimental session measured a threshold for a particular orientation, so that the orientation of all patterns remained constant during each session. Different orientations were set for different sessions by physically rotating the display, which was a 4 deg circular field set in a 12 deg circular surround matched in hue and brightness to the central display field. The orientation for each session was chosen in an irregular order separately for each observer and task. Observers in both experiments were seated 150 cm from the stimulus screen. Head stabilization was achieved by a chin and forehead rest modified to also include bilateral head supports.

Spatial frequency task

In the case of the spatial frequency discrimination experiments sinusoidal gratings were displayed at 30% contrast. Each session employed a constant reference frequency and a set of nine test frequencies chosen symmetrically around the reference. Each trial consisted of a .75 sec presentation of one of the grating, a .75 sec interstimulus interval, and a .75 sec presentation of one of the test gratings. Spatial phase was randomized on each presentation for both reference and test gratings independently. The order of test presentations was randomized according to the method of constant stimuli and each test pattern was presented 50 times. Following each trial the observer indicated whether the test frequency was higher or lower than the reference and was given feedback by synthesized voice indicating the true relationship. The probability distributions were fit to a cumulative normal distribution and the just noticeable difference (jnd) in frequency (Δf) was defined as the change in frequency necessary to increase the probability of a correct response from .5 to .75. The fitting procedure also estimated the statistical error in Δf.

Vernier offset task

The vernier offset experiments were identical in all respects to the spatial frequency discrimination experiments except that each presentation of a grating was replaced by the presentation of a vernier discrimination target consisting of two narrow line segments each .25 deg long separated by a gap of .25 deg. For the reference pattern the two lines were collinear while the test patterns had small perpendicular offsets. The overall position of the target was randomly offset from the center of the screen for the test and reference patterns independently on each trial by up to .2 deg. The task of the observer was to determine the direction of the vernier offset, and the jnd in offset (Δo) was determined as for Δf. Orientation for different sessions was again varied by physically rotating the screen.

FINDINGS FOR OBJECTIVE 2:

Spatial-discrimination and 2-dot vernier acuity show both a square component (90 degree bias) as well as a hexagonal component (60 degree bias) as a function of stimulus orientation

Spatial frequency

The results of the spatial frequency experiments are shown on the top of Fig. 5 for observer SC at a reference frequency of 4.0 c/deg and for observer JH at a reference frequency of 4.5 c/deg. The figure shows the fractional jnd in spatial frequency $\Delta f/f$ (f is the reference frequency) plotted against the orientation of the grating where an orientation of 0^o corresponds to the usual vertical grating. The data are clearly not constant but show significant variation with orientation. Multiple data points are repeated measurements over time and show good ·tability.

Vernier

The bottom of Figure 5 shows the results for the vernier discrmination experiments for the same two observers with the gap in the vernier target equal to .25 deg, also chosen in the expectation of a maximal hexagonal offset. The vernier offset thresholds are plotted against the orientation of the stimulus with an orientation of 90^o corresponding to the usual vertical vernier target. This choice is not arbitrary but is required to align the vernier discrimination data with the spatial frequency discrimination data. The vernier thresholds also clearly depend on orientation and are stable over time as indicated by multiple determinations.

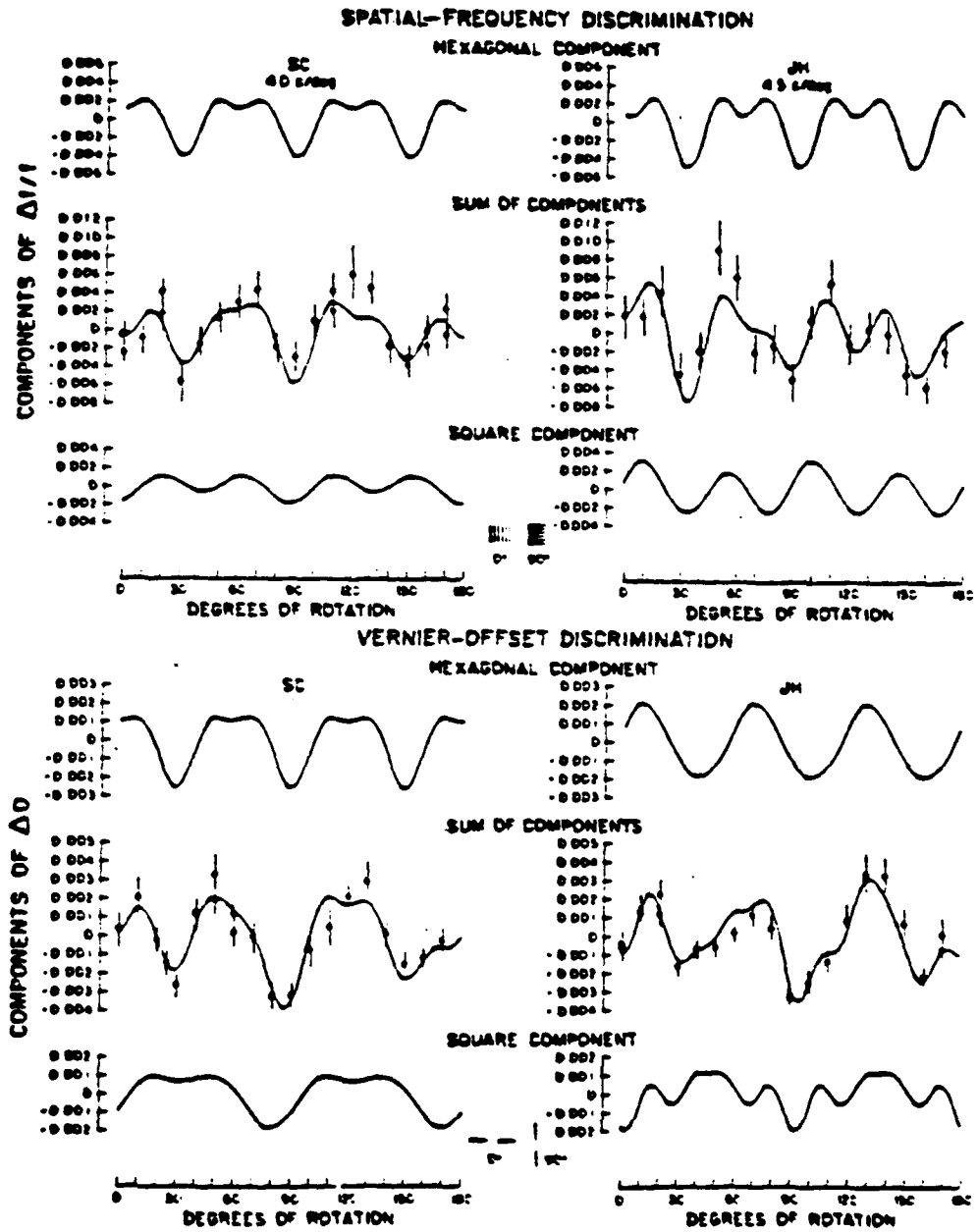

Fig 3. The decomposition of orientation dependence into hexagonal and square components for the spatial-frequency-discrimination task (upper sections) and for the vernier-offset-discrimination task (lower sections). Center plot in each quadrant shows the sum of hexagonal and square components plus the data reprinted from Figs 1 and 2 (minus the average). Note that 0° rotation is a vertical spatial-frequency grating (top graphs) and a horizontal vernier-line segment (bottom graphs).

Figure 5. From: Hirsch, J. and Hylton, R. (1984) 'Orientation dependence of hyperacuity contains components with hexagonal symmetry.' J. Opt. Soc. Am. A. 1, 300-308.

We find that the orientation dependence of the data presented above consists of the sum of two periodic components, one with hexagonal symmetry (60° period) and harmonics thereof and the other with square symmetry (90° period) and its harmonics.

The decomposition of the total orientation dependence into hexagonal and square components is shown by the smooth lines (Figure 5). The middle plot in each of the four parts shows the fit to the hexagonal + square model. Immediately above and below each fit is separately plotted the hexagonal and square component respectively. There are a number of noteworthy features. First, the phase of the hexagonal components are fairly closely aligned across tasks and across observers, having a minimum near 90o. While this orientation represents a vertical vernier target, the corresponding grating is horizontal. This is an important observation since it demonstrates that the orientation on which the hexagonal component primarily depends is not the orientation along which the jnd is being measured (the jnd's are measured along orthogonal directions for vertical vernier targets and horizontal gratings) but some other direction, and a possible explanation is given below. The square component for the vernier data also has a minimum near 90° (and 0°). The square components for the spatial frequency data (which are oly marginally statistically significant) seem to be more octagonal (period = 45°) than square.

The results above show that a model consisting of the sum of a hexagonal plus a square component, each with even symmetry, is sufficient to explain the observed orientation functions reported here, and both components are necessary within this model. The necessity of the hexagonal and square components can also be established in a very strong model independent manner, leading to the conclusion that it is essentially impossible for any model which lacks either component to fit the data.

These results demonstrate that the hyperacuity threshlds reported here display an orientation anisotropy having components with both hexagonal and square symmetry. This effect cannot be an artifact since our display apparatus was circularly symmetric. Although a square component or 'oblique effect' is most often reported in spatial tasks as a function of orientation (Mitchell, Freeman and Westheimer, 1967, Matin and Drivas, 1979, Tyler, 1977, Appelle, 1972). Caelli *et al.* (1983) have recently reported spatial frequency discrimination data that also clearly show a strong 60o periodicity for one observer and what appears to be a mixture of 60° and 90° components for other observers.[12] Since in our study, two quite different tasks, spatial frequency discrimination and vernier offset discrimination, both show a hexagonal component we conclude the underlying cause must be general. Extending arguments made previously, we attribute the hexagonal orientation anisotropy of hyperacuity to the existence of a cortical representation of an image, which we refer to as a neural lattice, that preserves the hexagonal symmetry of the retinal photoreceptor lattice.

OBJECTIVE 3: TO DETERMINE THE LIMITS OF SPATIAL-FREQUENCY DISCRIMINATION FOR VERY LOW SPATIAL FREQUENCIES.

Previously we reported that the ability of human observers to discriminate between different spatial frequencies was not a smooth function of frequency but rather had a definite segmented structure.4 We interpreted this structure as being due to reconstruction of the images on a set of cortical lattices with discrete effective spacings of ε/N where ε was found to be the foveal lattices with photoreceptor spacing (~ 0.008 deg) and N was an integer factor attributable to cortical interpolation. However these previous results were restricted to spatial frequencies above 2 cycles/degree (c/deg) and our model did not deal with lower frequencies. In this study we extend our measurements to frequencies as low as 0.3 c/deg and the model to all visually accessible spatial frequencies.

Methods and Procedures for Objective 3

The methods used are identical to those previously described except that the gratings consisted of narrow bright lines on a dark background rather than suprathreshold sinusoidal gratings. Briefly, each experimental session employed a fixed reference frequency and either 7 or 9 test frequencies chosen symmetrically around the reference frequency. Each trial consisted of the presentation of a reference grating for 0.75 sec, an interstimulus interval of 0.75 sec, and a test grating for 0.75 sec. The observer responded by indicating whether the test grating had a higher or lower spatial frequency than the reference. Following each response a synthesized voice indicated the correct choice. The test and reference phases were independently randomized on each trial and test frequencies were randomized together according to the method of constant stimuli. There were usually 50 trials per test stimulus and at least 40. Distance from the observer to the display, a Tektronix 606 monitor, was varied so that there were always at least 3 lines on the screen. Head stabilization was achieved by adjustable chin and forehead rests with snug cushions on both sides of the head. Viewing was central but with no explicit fixation target. The data from each session were fit to a cumulative normal distribution to determine the just noticeable difference (jnd) in frequency Δf, defined as the change in frequency necessary to raise the probability of a correct response from 0.5 to 0.75. The fitting procedure also provided an estimate of the statistical error in Δf for each session. Following our previous work, we consider the separation between bars $s = 1/f$ as the critical stimulus, not f. However in what follows we will generally use f and s interchangeably. Further, we have shown that $\Delta s/s = \Delta f/f$, and note that the inverse of separation is dimensionally the same as spatial frequency.

FINDINGS FOR OBJECTIVE 3:

<u>Low spatial-frequencies between 0.3 and 2.0 c/deg are similarly segmented.</u> <u>However</u>, the fundamental sampling unit appears to <u>larger</u> than the photoreceptor center-to-center spacing

Figure 6 shows the results of this experiment for four observers: GC. CS. SC and SG. The fractional jnd in spatial separation $\Delta s/s$ is plotted against the inverse of spatial separation s where $s = 1/f$ is the distance between lines in the grating. The data are clearly not smooth functions of frequency but cluster around straight lines drawn through the origin, with transitions between the line segments occurring regularly at about every 0.6 ~ 0.7 c/deg. This segmented structure has been seen previously at higher spatial frequencies (above 2 c/deg) where the spacing between transitions was about 4 c/deg.

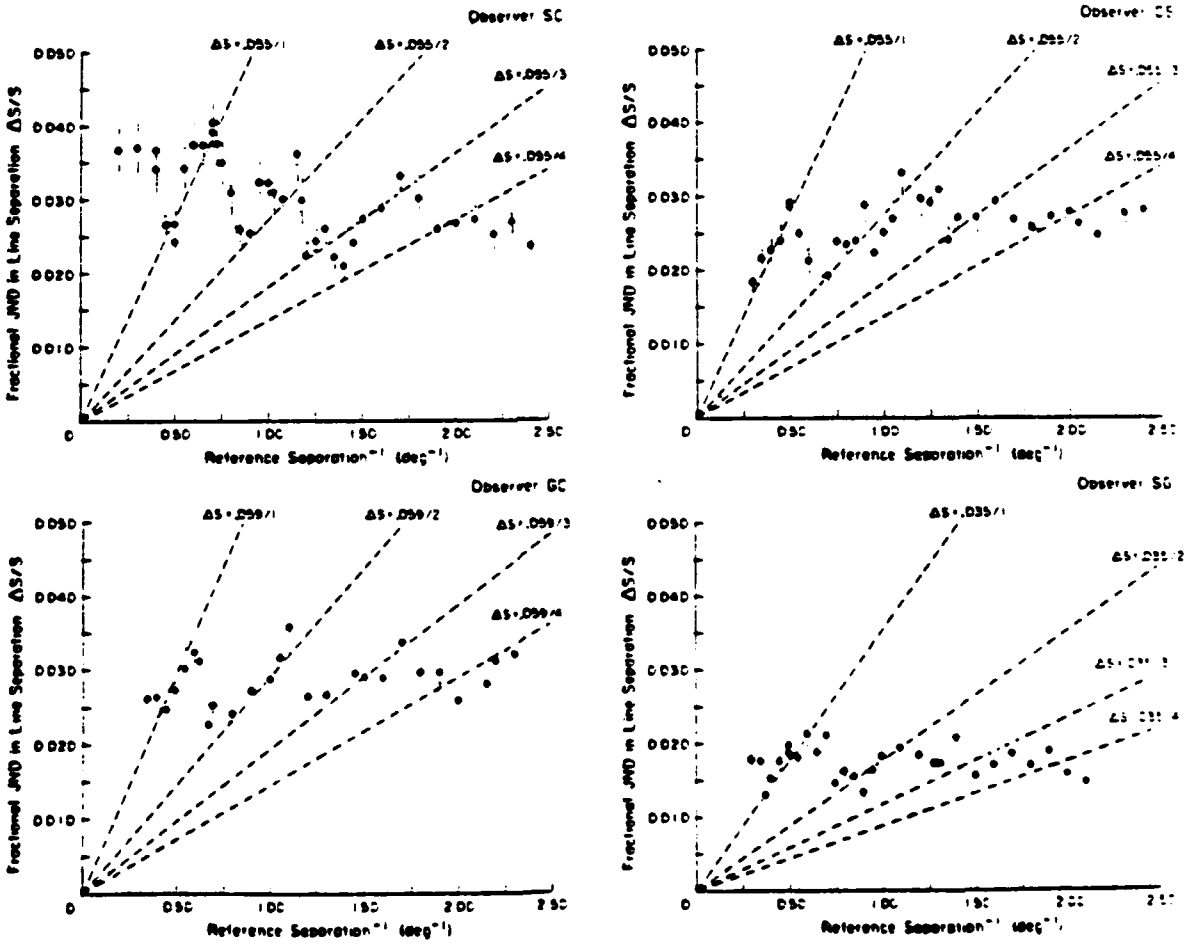

Fig. 1. Results of the line-grating spatial-frequency discrimination experiments for spatial frequencies between 0.3 and 2 c/deg. The fractional JND in separation $\Delta s/s$ is plotted against the inverse of reference separation, which is dimensionally equivalent to spatial frequency. Data are shown for four observers, GC, CS, SC, and SG. The slopes of the dashed lines drawn through the segments are shown as $\Delta s = c/N$ deg, and the error bars drawn through the data are explained in the text. The complete set of data is fitted to a smooth periodic function (dotted line) by allowing a smear from segment to segment. Results of the fit are given in Table 1.

Figure 6. From: Hirsch, J. and Hylton, R. (1985) Spatial-frequency discrimination at low frequencies: evidence for position quantization by receptive fields J. Opt. Soc. Am. A. 2, 128-135.

As shown in our previous work a straight line passing through the origin in the $\Delta f/f$ vs f plane is a region in which the jnd in spatial interval Δs is constant. Thus the segments of slope ε/N are regions in which there is a constant spatial jnd $\Delta s = \varepsilon/N$. Following our previous work we attribute each segment to the existence of a cortical lattice with effective spacing ε/N. For $N = 1$ the cortical lattice has the same effective spacing as the retinal spatial sampling lattice while the higher N lattices are constructed by interpolating between the retinal samples onto a cortical lattice with a spacing N times finer than the spacing of the retinal lattice. This scheme represents a highly efficient use of the retina to cortex connections.

For the high frequency band (above 2 c/deg) the fundamental spacing ε was found to be about 0.008 deg or one photoreceptor. N may be as high as 8 (taking ~32 c/deg as the high frequency limit), although it would be very difficult to prove that all the intermediate values of N exist. For the frequency band from 0.3 to 2 c/deg (which we call the mid-frequency limit), ε is about 0.0056 deg or 7 times the spacing of the photoreceptor and N goes from 1 to 4. We attribute this value of ε to the existence of a class of retinal receptive fields, the mid-frequency spatial sampling fields, which have a center-to-center spacing of 0.056 deg. These fields have two functions. First, they perform a spatial sampling function analogous to that of the photoreceptor, reducing a continuous luminance distribution to a finite number of measurements per unit interval for transmission to the cortex, but on a larger scale and thus drastically reducing the number of fibers required in the optic nerve. However, cortical interpolation between samples is impossible unless the image is sufficiently blurred to excite at least three sample points (in one dimension) (Barlow, 1979, Westheimer, 1979, Fahle and Poggio, 1981). For the high spatial frequencies this blurring is performed by the optics of the eye (Campbell and Green, 1965). For the mid-frequency band the blurring must be accomplished neurally by overlapping the spatial sampling fields to a considerable extent. Thus the widths of the fields must be several times their center-to-center separation or about 0.1 ~ 0.2 deg full width at half maximum for the excitatory center (Barlow, 1964). This is in reasonable agreement with previous psychophysical estimates of receptor field sizes. For example, Wilson and Gelb propose a model having a discrete set of 6 receptive field sizes of which one has a center spacing of 0.055 deg (with a 0.25 octave observer to observer variation) and another has a center spacing of 0.047 deg, both quite comparable to the values reported here (Wilson and Gelb, 1984). The receptive field widths estimated by Wilson and Gelb (1984) are also comparable to our somewhat poorly constrained estimates.

OBJECTIVE 4: TO INVESTIGATE THE QUALITY OF THE PRIMATE PHOTORECEPTOR LATTICE AND RELATE THE STRUCTURAL PROPERTIES OF THE FOVEAL RETINAL MOSAIC TO THE 'NEURAL METRIC' EMPLOYED IN HYPERACUITY TASKS.

To study the question of photoreceptor lattice quality we have analyzed the foveal cone mosaic from an adult primate (Macaca fascicularis) using a section taken tangent to the external limiting membrane (ELM) close to its scleral side (Miller, 1979). This section as shown in Figure 7.

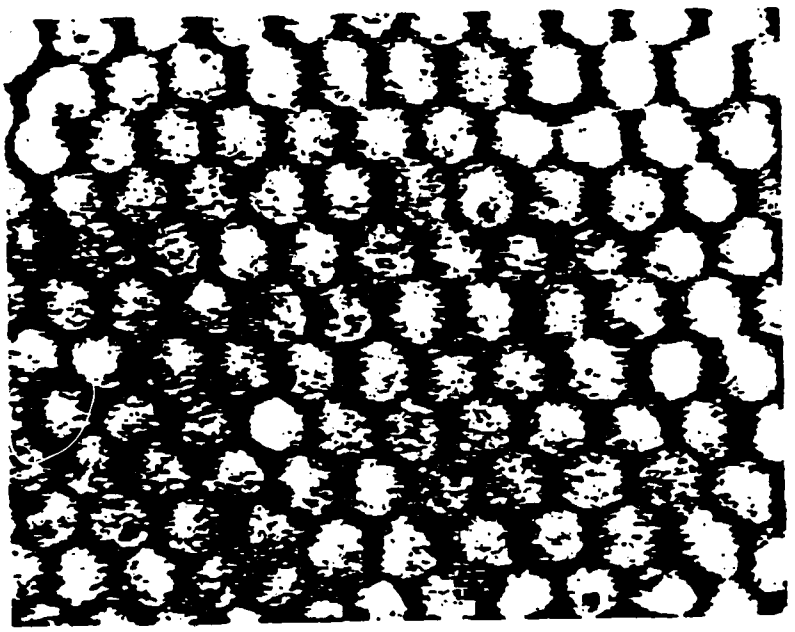

Fig. 7. Cone inner segments at the central fovea in the retina of the monkey. Macaca fascicularis shown in a photograph of a 1 um thick section tangent to and on the scleral side of the external limiting membrane. Center-to-center distance of cones is 3 um. From Miller (1979) with permission.

Figure 7. From: Hirsch, J. and Hylton, R. (1984) 'Qualtiy of the primate photoreceptor lattice and limits of spatial vision.' Vision Res. 24, 347-355.

Methods and Procedures for Objective 4

Our analysis is based on measurements of the positions of the centers of about 100 cones inner segments in the central fovea. This lattice was chosen for analysis rather than that published by Polyak (1957) and studied by Yellott (1982) because the Polyak lattice is a photograph of a whole mount that appears to be focused near the level of the outer segments. The outer segment locations are irrelevant for positionial analysis since the outer segments are basically light guides for photons that enter the cones at the inner segments. The outer segments may also be subject to substantial positional distortion since they are embedded in a semifluid extracellular matrix. In contrast, the positions of the inner segments are fixed at the ELM by desmosomes, after which they taper and increase in refractive index to become light guides, providing the mechanism by which the cones form separate optical channels. Thus the inner segment at the ELM is the spatial

aperture of the cone for its photon catching function and its position specifies cone location for the purpose of image reconstruction. We further note that the Miller lattice displays clearly higher spatial quality than the Polyak lattice. Given the unlikelihood of accidentally introducing order into an initially disordered lattice, the more orderly lattice must be more representative of the intact retina.

FINDINGS FOR OBJECTIVE 4:

<u>The primate foveal photoreceptor lattice is a highly regular hexagonal array of cones</u>

Figure 8 shows a histogram of the distances between the centers of all pairs of photoreceptors in our sample. There is a very distinct peak corresponding to the nearest neighbor distance (which we call ring 1). The rms width of the peak (standard deviation of the nearest neighbor distance) is .077 times the mean separation between nearest neighbor photoreceptors and drops to .070 when the contribution from our measurement error is removed. This is comparable to the maximum tolerable spacing error (.078) estimated below from human psychophysical results.

Figure 9 shows a histogram of the angles between the horizontal axis and the lines connecting the center of each photoreceptor to the center of its nearest neighbors where nearest neighbors are defined as any pair whose center to center separation is less than the maximum nearest neighbor distance shown in 8a. This figure shows a well defined set of direction with hexagonal symmetry (60^{o} spacing) which determine the orientation of the lattice, and is consistent with previous qualitative observations of retinal structure (Borwein et al., 1980, Polyak, 1957).

By specifying the mean nearest neighbor distance and orientation of the lattice we have fully determined the basis vectors for the lattice (Kittel, 1971). We then make the following calculations. For each photoreceptor we take its center to be the origin and use the nearest neighbor distance cut to locate its nearest neighbors. We then measure the difference between expected and actual positions for the photoreceptors just assinged to the ring of nearest neighbors assuming a perfect hexagonal lattice with the basis vectors determined above. The nearest neighbor distance cut is then used again to move out from the nearest neighbors to the ring of second nearest neighbors and again we measure the error in actual position versus the expected position for a perfect hexagonal lattice centered on the original photoreceptor. We continue this process until all photoreceptors have been assigned to soe ring and their errors computed. The process is then repeated with a new photoreceptor at the origin. Figure 9 shows a graph of the variance (mean square error) in relative position as a function of ring number. The data have been normalized so that the mean nearest neighbor photoreceptor distance (ring 1) is 1.0. We plot separately the components of variance parallel and perpendicular to the line which joined the photoreceptor at the origin and the one being tested. The parallel component corresponds to errors in separation while the perpendicular component corresponds to errors in orientation. The variance increases linearly with distance (ring number), consistent with accumulating uncorrelated errors, and the parameters of the best fit straight lines are given in Table I.

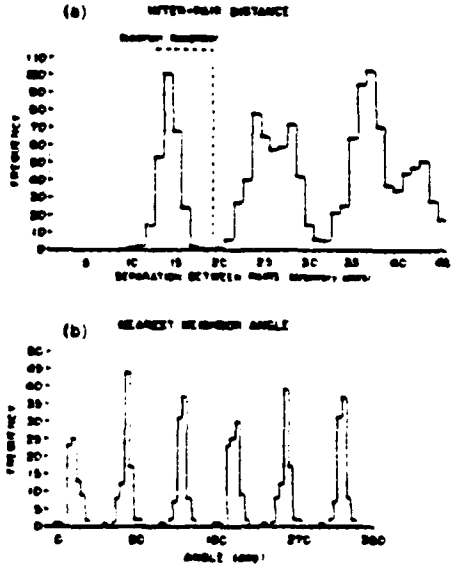

Fig 2 (a) Histogram of distances between all pairs of photoreceptors in the sample shown in Fig 1. The first peak shows the distribution of distances between the centers of nearest neighbors (b) Histogram of all angles between the horizontal axis and the lines connecting the center of each photoreceptor to the center of its nearest neighbors. The six peaks demonstrate a high quality hexagonal lattice.

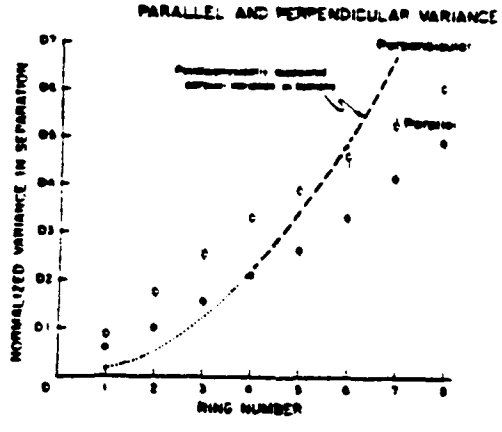

Fig 3 Variance between expected and actual positions of photoreceptors vs ring number normalized so that the nearest neighbor distance is 1.0 Solid circles correspond to errors in separation (parallel) and open circles correspond to errors in orientation (perpendicular) The curve is a psychophysical estimate of the total parallel variance in spatial interval measurement by humans

Figures 8 and 9. From: Hirsch, J. and Hylton, R. (1984) 'Quality of the primate photoreceptor lattice and limits of spatial vision'. Vision Res. 24, 347-355.

If we define the positional correlation length of the lattice as the distance between two lattice points at which the rms spacing eror equals the lattice spacing, then the correlation length for the parallel component is 178 ± 7 photoreceptors and for the perpendicular component the correlation length is 133 ± 5 photoreceptors.

Table 1

Parameters of Best Fit Lines

Variance* vs Ring Number

Variance*	Slope	Intercept	X^2	df	Conf.
Uncorrected					
parallel	.0056 ± .0002	.0001 ± .0006	8.89	6	.18
perpendicular	.0075 ± .0003	.0021 ± .0009	2.60	6	.86

*Variance is expressed in units of square mean inter-neighbor distance.

The fundamental spacing error of the lattice is matched to the psychophysical limits of positional uncertainty

The first isolated distribution in Figure 8a is the distribution of distances of all nearest neighbors. Normalized so that the mean distance, $\bar{d}$, is 1.00, the RMS for that distribution is .07 ($\bar{d}$). This width is the fundamental spacing error of the lattice.

The psychophysical limits of positional uncertainty for interval discrimination tasks is determined from a cummulative normal fit to the psychometric function where a jnd is defined as the range of test separations within 0.68 standard deviations. Two important observations for this argument are shown in Figure 4: 1) over-all (disregarding the fine structure of the spatial frequency discrimination function) the fractional jnd is constant at about 0.025, and 2) the limit of spatial frequency discrimination is about 28 c/deg.

The following argument relates the lattice error and positional uncertainty of the visual system.

1. The fractional jnd in spatial frequency is equivalent to the fractional jnd in separation:

$$\frac{\Delta f}{f} = \frac{\Delta s}{s}$$

argument:

a) separation = 1/frequency
$s = 1/f$

b) differentiating# (minus sign is neglected since it has no meaning in this context)

$$\Delta s = \Delta f / f^2$$

c) rearranging terms:

$$\Delta s f = \Delta f / f$$

Note: this equation is a straight line passing through the origin when Δs is constant

d) substituting for f:

$$\Delta s / s = \Delta f / f$$

2. Fractional jnd = 0.025. See Figure 4.

$$\Delta s = 0.025\ (s)$$

3. Convert the jnd Δs to standard deviation units σs.

$$\sigma s = \left(\frac{0.025}{0.68} \right) s$$

$$\sigma s = 0.037\ s$$

4. At the limits of spatial frequency discrimination (28 c/deg)
$s = 0.04$ deg (1/28 degree)

$$\sigma s = 0.037\ (.04 \text{ deg})$$

5. A separation of 0.04 deg is equivalent to the distance subtended by 4.5 photoreceptors ($d_{cc} = 0.008$ deg)

6. Assume that spacing errors accumulate proportionally to the square of distance

$$\sigma s = 0.037\ \ 4.5$$
$$= 0.078$$

7. Therefore the lattice spacing error, 0.07, determined above is reasonably matched to the psychophysical limits of positional uncertainty 0.078.

Note: This argument is presented in more detail in Hirsch and Hylton, 1984.

OBJECTIVE 5: TO DEVELOP A MODEL OF SPATIAL DISCRIMINATION BASED ON SPATIAL PROPERTIES RATHER THAN CONTRAST.

1. The scaled lattice model for spatial tasks involving geometrical judgements was proposed based on the photoreceptor lattice as the fundamental 'ruler' for spatial vision

We present here an outline of the scaled lattice model of spatial vision. The development of the model is in an early stage and there are major aspects which need to be further addressed experimentally. Notably, we neglect binocular vision, two dimensional considerations, temporal effects, and the interaction between multiple simultaneously present spatial scales. However the following provides a listing of some important elements and a basis for future development.

a. Retinal images are optically blurred and sampled by photoreceptors. In the central regoin of the retina the output of each photoreceptor (perhaps after convolution with some local weighting function designed to remove low frequencies) is then transmitted to the cortex for further processing. Over the central and larger regions photoreceptors are pooled into regularly spaced spatial sampling fields with overlapping excitation functions designed to remove high frequencies and provide sufficient neural blurring to allow interpolation between field centers. Only one output per spatial sampling field is transmitted to the cortex. There are presumably a sequence of classes of spatial sampling fields of increasing center-to-center spacing with the spatial extent covered by each class presumed proportional to the spacing of that class. That is, the optic nerve per each photoreceptor sampling and all the classes of receptive field sampling coexist in the central part of the retina but the coarser samplings extend to greater eccentricities. The point of this scheme is to efficiently encode the position information in the retinal image by sampling near the sampling limit for multiple scales of sampling allow more detail to be encoded at smaller eccentricities.

b. The image is reconstructed in the cortex for a given sampling scale by interpolating between sample points onto a neural lattice whose spacing is an integer (N) times finer than the sample spacing. Note that there is no information in this reconstruction that was not present in the original sampling. The neural lattice (with $N > 1$) basically represents an unpacking of the highly encoded information in the original sampling into a form in which the position information is more accessible, with higher values of N allowing more detailed unpacking and hence more accurate localization of the features of the image. The interpolation may include convolution with a function designed to enhance some aspect of the image or to remove frequencies too low to be of interest. The total spatial extent of each lattice is assumed proportional to the effective lattice spacing, resulting in an apparent inverse cortical magnification factor that is a roughly linear function of eccentricity.

c. The positions of local features such as peaks or perhaps points of inflection are determined to the nearest lattice point by comparing neighboring points in the neural lattice. For example, peaks can be localized by testing three successive points to see if the sign of the slope has changed.

d. Spatial intervals are measured by counting points in the neural lattice between the features located above. Assuming the localization procedure is sufficiently accurate, the error (jnd) in the spatial interval will then be dominated by the effective spacing of the neural grid. Thus the neural lattices, which are derived from the photoreceptor lattice, serve as rulers of differing scales for the measurement of spatial intervals (Hirsch and Hylton, 1984a and b).

e. There exists an automatic scale selection mechanism which chooses the sampling scale and interpolation factor such that the effective lattice spacing i roughly proportional to the spatial scale of the measurement. Thus $\Delta s/s$ is rough constant, where Δs is the spatial resolution and s is the spatial scale. The motivation of this scaling is to keep the total number of elements required at a tractable number independent of the image size.

Figure 10 is an illustration of the scaled lattice model. For clarity we show only the fundamental photoreceptor sampling and a 3:1 interpolation. Part a) shows the external luminance distribution, a delta function. Part b) shows the luminance distributin after blurring, and c) shows the sampling of the image by the photoreceptors. Part d) represents the interpolation process, which accepts the coarsely sampled input from the photorecpeotrs and produces a more finely spaced sampling on the neural lattice (e). We have drawn the neural unit spacing as 1/3 the photoreceptor spacing, but in general it can be 1/N where N is an integer. Part f) illustrates local feature detection on the neural unit lattice, showing a peak detector (square) receiving input from three adjacent neural units. Part g) is a possible realization of a position independent separation detector using pre-counted intervals for speed. The separation detector performs the function Peak (x) and Peak (x + s) ORed over all x, and would have many properties usually attributed to spatial frequency selective channels with spatial summation.

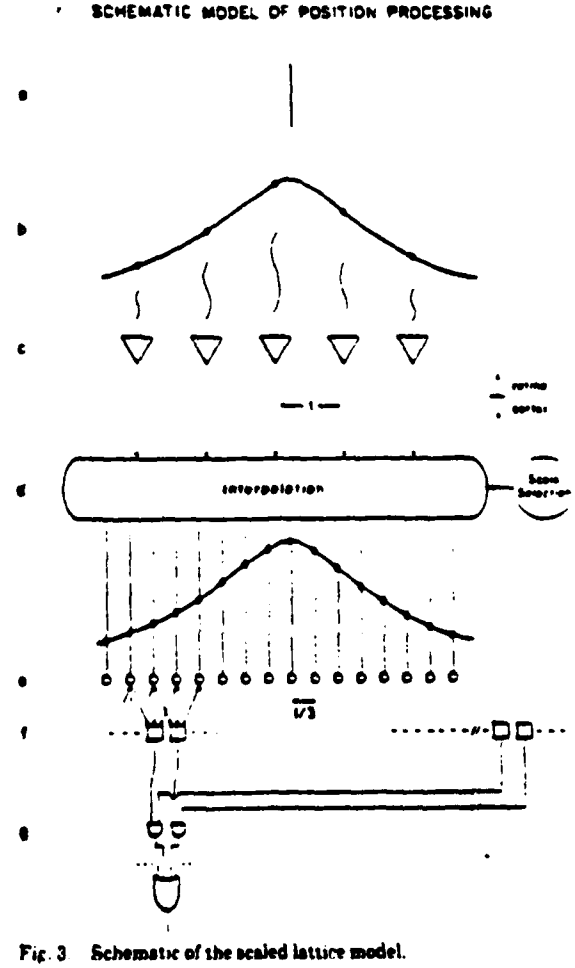

Fig. 3 Schematic of the scaled lattice model.

Figure 10. From: Hirsch, J. and Hylton, R. (1984) 'Orientation dependence of hyperacuity contains components with hexagonal symmetry.' J. Opt. Soc. Am. A. 1, 300-308.

3. List of Publications from AF Contract

Hirsch, J. and Hylton, R. Limits of spatial-frequency discrimination as evidence of neural interpolation. J. Opt. Soc. Am. 72:1367-1374, 1982.

Hirsch, J. and Hylton, R. Quality of the primate photoreceptor lattice and limits of spatial vision. Vision Res. 24:347-355, 1984.

Hirsch, J. and Hylton, R. Orientation dependence of visual hyperacuity contains components with hexagonal symmetry. J. Opt. Soc. Am. 1:300-308, 1984.

Hirsch, J. and Hylton, R. Spatial frequency discrimination at low frequencies: evidence for position quantization by receptive fields. J. Opt. Soc. Am. A. 2:128-135, 1985.

Hirsch, J. Line-separation discrimination curve in the human fovea: smooth or segmented: A reply to Gerald Westheimer. J. Opt. Soc. Am. A. 2:477-478, 1985.

Hirsch, J. and Miller, Wm. H. (1985) Irregularity of foveal cone lattice increases with eccentricity. Supplement to Investigative Ophthalmology and Visual Science 26, p. 10.

Groll, S.L. and Hirsch, J. (1985) Shifts in Spatial discrimination within 2 degrees of retinal eccentricity. Supplement to Investigative Ophthalmology and Visual Science 25, p. 145.

Groll, S.L., Hirsch, J., Hylton, R. and Miller, Wm. H. (1984) Photoreceptor lattice and spatial vision: the effect of eccentricity. Supplement to Investigative Ophthalmology and Visual Science 25, p. 145.

Hirsch, J. and Hylton, R. (1984) Spatial-frequency discrimination at low frequencies: evidence for spatial quantization by receptive fields. Supplement to Investigative Ophthalmology and Visual Science 25, p. 52.

Hirsch, J. and Hylton, R. (1983) Quality of the photoreceptor lattice limits spatial vision. Technical Program 1983 Annual Meeting: Optical Society of America p. 11.

Hirsch, J. and Hylton, R. (1983) Oreintation dependence of hyperacuity contains components with hexagonal symmetry. Supplement to Investigative Ophthalmology and Visual Science 24, p. 276.

Hirsch, J. and Hylton, R. (1982) Spatial frequency discrimination of suprathreshold gratings. Supplement to Investigative Ophthalmology and Visual Science 22, p. 271.

Hirsch, J. and Hylton, R. Two dimensional sampling by the retinal lattice. Technical Report no. 8303. Medical Imaging Division. Yale University School of Medicine. 1983.

Hirsch, J. and Hylton, R. A model for the processing of position information in the human visual system. Technical Report no. 8304. Medical Imaging Division, Yale University School of Medicine. 1983.

Papers Submitted

Hirsch, J. and Groll, S.L. Vernier offset discrimination vs. Gap size obeys Weber's Law. Submitted, 1986.

Groll, S.L. and Hirsch, J. Two-dot vernier discrimination declines within 2.0 degrees of the foveal. Submitted, 1986.

4. List of Professional Personnel

1. Joy Hirsch, Ph.D. Associate Professor, PI

2. John Rose, Systems Analyst, Programmer

3. Cathryne Stein, Laboratory Assistant

   Elisa Manalo, Laboratory Assistant

   Kathy Granfield, Laboratory Assistant

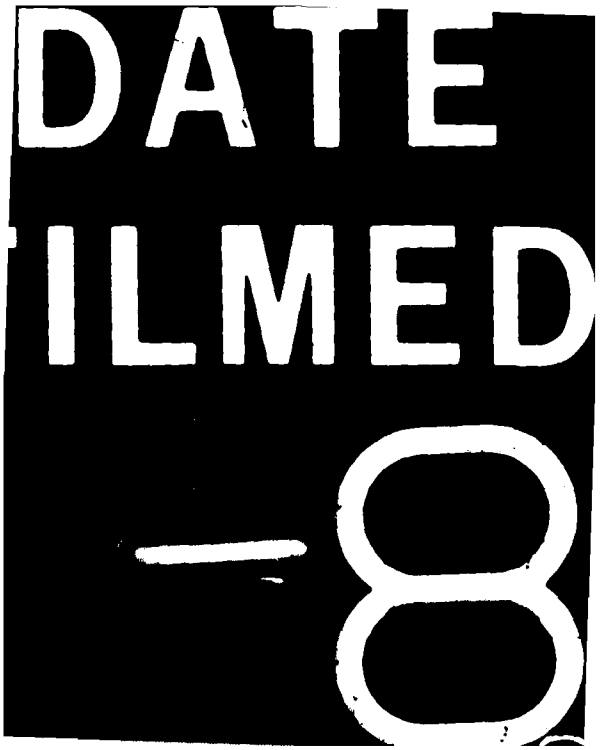
DATE
ILMED
-8